Soft Matter

RSC Publishing

PAPER

View Article Online
View Journal | View Issue

Cite this: *Soft Matter*, 2013, **9**, 6046

Enhancing and reversing the electric field at the oil–water interface with size-asymmetric monovalent ions

Guillermo Iván Guerrero-García,[a] Yufei Jing[a] and Mónica Olvera de la Cruz*[ab]

The electric field at the interface between two immiscible electrolyte solutions determines the self-assembly of synthetic and biomolecular nanoparticles at liquid interfaces and the physical properties of important biological and technological processes such as drug delivery, stability of emulsions or electro-extraction of metal ions from industrial wastewater. The classical Poisson–Boltzmann theory has been widely used to describe the corresponding ionic distribution, even though it neglects the polarization and ion correlations typical of these charged systems. Here, using Monte Carlo simulations, we provide an enhanced description of an oil–water interface in the presence of an electric field without needing any adjustable parameter, including realistic ionic sizes, ion correlations, and image charges. Our data agree with experimental measurements of excess surface tension for a wide range of electrolyte concentrations of LiCl and TBATPB (tetrabutylammonium-tetraphenylborate), contrasting with the result of the classical non-linear Poisson–Boltzmann theory. More importantly, we show that the size-asymmetry between small Li^+ and large Cl^- ions can significantly increase the electric field near the liquid interface, or can even reverse it locally, at high salt concentrations in the aqueous phase. These observations suggest a novel trapping/release mechanism of charged nanoparticles at oil–water interfaces in the vicinity of the point of zero charge. In the absence of an applied electric field, a difference in the mean electrostatic potential in the bulk phases of both immiscible electrolytes due to ion partitioning would also promote similar effects in synthetic and biomolecular liquid interfaces.

Received 15th March 2013
Accepted 17th April 2013

DOI: 10.1039/c3sm50753j

www.rsc.org/softmatter

The ionic cloud at the interface between two immiscible electrolyte solutions (ITIES) is the so-called electrical double layer. This accumulation of diffuse charge can arise from the difference in the ionic solvation energy in each liquid medium or from the application of an electric field. In living organisms, different dielectric properties and ion concentrations can be maintained inside cells in contrast to the external medium *via* molecular pumps, which can induce transmembrane ion diffusion metabolizing energy. The molecular details of the ionic distribution near the ITIES determine the properties of the electric field generated by these charged particles. The relevance of the electric field (or the electrostatic interactions) to the adsorption and self-assembly properties of charged colloidal micro/nanoparticles at liquid interfaces has been demonstrated in recent experimental studies as a novel avenue to design more complex molecular structures.[1,2] In fact, colloidal nanoparticles can be used to stabilize emulsions producing so-called microcapsules,[3] which could be used to deliver encapsulated materials in biomedical applications. Label-free detection based on liquid–liquid interfaces has also been proposed.[4] In addition, the electric field has been related to the proper performance of biological functions at the cellular level,[5,6] displaying the ability to accelerate or improve wound healing when it is applied externally.[7] The knowledge of the electric field at liquid interfaces is also crucial for the development of enhanced devices to store energy safely and efficiently, such as double layer supercapacitors,[8] or to improve the ion transfer and electro-assisted solvent extraction of metal ions from wastewater and industrial fluids.[9]

In order to gain a better understanding of the molecular structure of the ITIES, simulation studies have been conducted considering explicitly solvent particles (see *e.g.*, ref. 10). Nevertheless, the vast number of solvent particles required to study the ITIES under experimental ion concentrations (typically in the range of millimoles) makes this kind of calculation non-attainable, despite the current advances in computing capability. On the other hand, the classical Poisson–Boltzmann theory of point ions has been used since last century to describe the electrical double layer at the ITIES.[11] One important limitation of this approach is that it does not take into account the ion correlations and excluded volume effects.[12,13] The former is related to the physical fact that an ion likes to be surrounded by ions of opposite charge, whereas the latter means that two ions cannot occupy exactly the same position in space. In the classical Poisson–Boltzmann theory of point ions, the two double layers that meet at the ITIES do not interact (that is, they are

[a]*Department of Materials Science and Engineering, Northwestern University, Evanston, IL 60208, USA. E-mail: ivan-guerrero@northwestern.edu; m-olvera@northwestern.edu*
[b]*Department of Chemistry, Northwestern University, Evanston, IL 60208, USA*

independent), and the corresponding polarization effects due to dielectric heterogeneities are completely neglected.[11] These effects are relevant if the dielectric properties of the two immiscible liquids in contact significantly differ. In the most simple case, polarization effects can produce the attraction (repulsion) of a single charge toward a macroscopic sharp interface limiting another medium with a higher (lower) dielectric constant.[14]

Given the evident limitations of the classical Poisson–Boltzmann picture of point ions, several theoretical approaches have been proposed to successfully describe the experimental results of the ITIES.[15–19] Nevertheless, these improved schemes are also restricted by ad-hoc adjustable parameters, which limits their predictive use. Thus, we perform here coarse-grained Monte Carlo simulations of an experimental oil–water interface in the presence of an electric field – including realistic ionic size-asymmetry, ion correlations, excluded volume of ions, and image charges – to study its thermodynamic and microscopic properties without needing any adjustable parameter. In particular, these Monte Carlo simulations are used to study the surface tension of oil–water interfaces in the presence of size asymmetric monovalent salts with the goal of determining the effects of ion correlations, polarization, and ionic excluded volume in the diffuse electrical double layer. At the molecular level, we observe that the electrolyte concentration and the ionic size-asymmetry can be used to tune the electric field near the liquid–liquid interface. Thus, the electric field can be significantly increased or even reversed in this region depending on the polarity of the difference in the mean electrostatic potential in the bulk phases of oil and water. We reproduce surface tension experimental data of LiCl and TBATPB (tetrabutylammonium-tetraphenylborate) near an oil–water interface in the presence of an electric field in the Results and discussion section. We use only experimental values of all relevant physical parameters of the system, such as the ionic size and the dielectric constant in the bulk liquid media, without any additional adjustable parameter. In the Conclusions section, we argue that the enhancement and the reversal of the electric field at high electrolyte concentrations is analogous to the surface charge amplification[20,21] and the charge inversion observed experimentally in macroscopic colloidal systems.[22–25] If a difference due to ion partitioning exists in the mean electrostatic potential in the bulk phases of oil and water, these phenomena could also be present in synthetic and biomolecular interfaces (*e.g.*, around cell membranes), even in the absence of an applied electric field.

I Model system and methods

We describe the ion distribution at the interface between two immiscible electrolyte solutions using the primitive model. In this scheme, the solvent is a continuum medium characterized by a dielectric constant, ε. Nitrobenzene and water, with dielectric constants $\varepsilon_O = 34.8$ and $\varepsilon_W = 78.4$, respectively, are the two immiscible adjacent solvents placed in contact. Ions are modeled as hard spheres with point-charges embedded in their centers. TBA^+, tetrabutylammonium, and TPB^-, tetraphenylborate, ions are submerged in nitrobenzene, while Li^+ and Cl^- ions are submerged in water. The diameter of the ionic species are: $d_{TBA^+} = 7.7$ Å, $d_{TPB^-} = 8.2$ Å, $d_{Li^+} = 4.2$ Å, $d_{Cl^-} = 6.4$ Å, for TBA^+, TPB^-, Li^+, and Cl^-, respectively.[26,27] The sharp dielectric discontinuity is modeled as an impenetrable neutral hard wall (see Fig. 1). We neglect the ion transfer between the two solvents because the standard Gibbs energies of transfer of LiCl from water to oil, and of TBATPB from oil to water are significant.[28] Polarization effects are included *via* the image charge method, as described below.

In typical experiments, an electric field is applied to the liquid–liquid interface. As a result, charge accumulation is observed on both sides of the dielectric discontinuity (see Fig. 1). Let us denote $E(\vec{x})$ as the electric field, and $\Psi_\infty^W - \Psi_\infty^O = \Delta_O^W\Psi$ as the difference in the mean electrostatic potential in the bulk phases of both immiscible electrolytes. The boundary conditions for this system are $\Psi_\infty^O = 0$ and $\vec{E}_\infty^O = 0$ in oil, and $\Psi_\infty^W = \Delta_O^W\Psi$ and $\vec{E}_\infty^W = 0$ in water. Physically, these boundary conditions establish that the difference in the mean electrostatic potential in the bulk phases of both electrolytes is constant, and the electric field vanishes in the bulk electrolytes. The original applied electric field in the experiments is replaced in our simulations by an imposed excess of surface charge density in nitrobenzene, σ_O, and water, σ_W (see Fig. 1). As the experimental system is electroneutral, the global excess charge imposed is equal to zero, $\sigma_W + \sigma_O = 0$. From the ion distribution around the liquid interface, it is possible to calculate the electric field near the dielectric discontinuity and the difference in the mean electrostatic potential in the bulk phases of the electrolytes, $\Delta_O^W\Psi$, for a given excess surface charge density in water, σ_W, using the Gauss law as described below. The advantage of this approach is that the specific details of the applied electric field producing the interfacial ionic accumulation are no longer required because, macroscopically, the electrodes are completely screened in the bulk phases of both immiscible

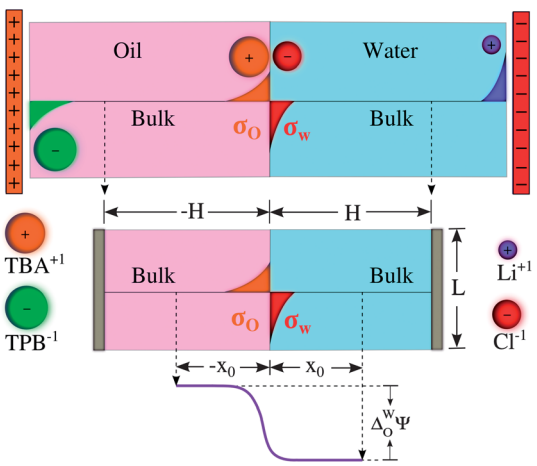

Fig. 1 Schematic representation of the experimental system (top), the Monte Carlo setup used in the simulations (middle), and the difference in the mean electrostatic potential in the bulk phases of both immiscible electrolytes (bottom).

electrolytes. Thus, the excess surface tension at the oil–water interface can be calculated as a function of $\Delta_O^W\Psi$ using the Lippmann equation:[29]

$$\sigma_W = -\frac{\partial\gamma}{\partial\Delta_O^W\Psi}. \quad (1)$$

A Electrostatic interactions in the presence of a dielectric discontinuity

In the primitive model, interactions among charged particles can be grouped into two types: one-body and two-body. These interactions can also be separated into a hard sphere contribution and an electrostatic component. The two-body interaction for hard spheres is given by $S_{ij}(r_{ij}) = 0$ if particles i (at position $\vec{r}_i = (x_i, y_i, z_i)$) and j (at position $\vec{r}_j = (x_j, y_j, z_j)$) do not overlap, and $S_{ij}(r_{ij}) = \infty$ otherwise. The distance between the particles is defined as $r_{ij} = \sqrt{(x_i - x_j)^2 + (y_i - y_j)^2 + (z_i - z_j)^2}$. We will denote α = O, W and β = O, W as the solvents in which particles i and j reside, respectively. These solvents have associated dielectric constants ε_α and ε_β. The two-body electrostatic interaction between particles i (with valence ν_i) and j (with valence ν_j) is given as

$$U_{ij}^{\alpha\beta}\left(\vec{r}_{ij}\right) = l_{\alpha\beta}\left(\frac{\nu_i\nu_j}{r_{ij}} + \frac{\varepsilon_\alpha - \varepsilon_{\alpha'}}{\varepsilon_\alpha + \varepsilon_{\alpha'}}\frac{\nu_i\nu_j}{r_{ij'}}\delta_{\alpha\beta}\right), \quad (2)$$

where α' is the complementary solvent to α, $\delta_{\alpha\beta}$ is the Kronecker delta, $l_{\alpha\beta} = \frac{e^2}{4\pi\varepsilon_0(\varepsilon_\alpha + \varepsilon_\beta)/2}$, e is the protonic charge, ε_0 is the vacuum permittivity, and $\vec{r}_{j'} = (-x_j, y_j, z_j)$ if the origin of the system is placed at the liquid interface according to the method of images.[14]

The one-body hard sphere interaction can be written as $S_i^\alpha(\vec{r}_i) = 0$, if LiCl ions are in water and TBATPB ions are in nitrobenzene, and there is no overlapping between the ions and the hard planes located at $x = -H$, $x = 0$, and $x = H$. Otherwise, $S_i(\vec{r}_i) = \infty$. This definition prohibits ion transfer between both solvents. The one-body electrostatic interaction is associated with the self-image electrostatic energy, which is defined as

$$U_i^\alpha\left(\vec{r}_i\right) = \frac{l_{\alpha\alpha}}{2}\frac{\varepsilon_\alpha - \varepsilon_{\alpha'}}{\varepsilon_\alpha + \varepsilon_{\alpha'}}\frac{\nu_i^2}{r_{ii'}}. \quad (3)$$

Here, α = O, W is the medium in which ion i is located, and α' is the complementary solvent.[14,30] The one-body and two-body interactions can be written as

$$H_i^{\text{one-body}}(\vec{r}_i) = S_i^\alpha(\vec{r}_i) + U_i^\alpha(\vec{r}_i) \quad (4)$$

and

$$H_{ij}^{\text{two-body}}(\vec{r}_{ij}) = S_{ij}(r_{ij}) + U_{ij}^{\alpha\beta}(\vec{r}_{ij}). \quad (5)$$

The total energy of the system is then defined as

$$H_T = \sum_{i=1}^{N} H_i^{\text{one-body}}\left(\vec{r}_i\right) + \frac{1}{2}\sum_{i=1}^{N}\sum_{j=1}^{N} H_{ij}^{\text{two-body}}\left(\vec{r}_{ij}\right), \quad (6)$$

where $i \neq j$, and N is the total number of particles. Electrostatics were properly included *via* the Torrie and Valleau's charged-sheets method[31] using Boda's modification.[32]

B Monte Carlo simulations of the liquid interface

In order to efficiently access concentrated electrolyte solutions, Monte Carlo (MC) simulations of the liquid–liquid interface are performed in the NVT ensemble. This approach has been discussed in detail in a previous study considering size-symmetric ions,[33] so we briefly sketch it here. A box of volume $2HL^2$ is used to perform the simulations (see Fig. 1). Periodic boundary conditions along the y- and z-directions, and a finite length of $2H$ along the x-axis are imposed. The sharp dielectric interface is modeled using an uncharged hard wall at the center of the simulation box at $x = 0$. This hard wall prevents ion transfer of TBATPB ions from oil to water and LiCl ions from water to oil. In addition, two impenetrable uncharged hard walls are located at $x = -H$ and $x = H$. The simulation box must be large enough to mimic a bulk electrolyte reservoir. We have monitored this condition, obtaining the desired bulk electrolyte concentration with an error of less than 1%. The total number of particles in the simulation box varied from 2000 for low electrolyte concentrations to 5000 for high electrolyte concentrations. In all instances, 50 000 MC cycles were performed to equilibrate the system. The canonical average was calculated using 900 000 MC cycles for low ion concentrations and 300 000 MC cycles for high ion concentrations.

C Calculation of the electric field and the surface tension

Let us consider a distance far enough from the dielectric discontinuity, at which the electrolyte can be considered in its bulk state. We denote this distance as x_0, which is shorter than half the length of the simulation box, H, in its finite dimension (see schematic representation in Fig. 1). In order to mimic the effect of an applied electric field in our Monte Carlo simulations, a number of TBA^+ or TPB^- ions are added to the bulk concentration of TBATPB in nitrobenzene. The corresponding excess surface charge density can be defined as

$$\sigma_O = \int_{-x_0}^{0} \sum_{i=TBA^+,TPB^-} \rho_i(x) e z_i \mathrm{d}x, \quad (7)$$

where $\rho_i(x)$ is the density of ions per volume unit of species i, and e is the protonic charge. Adding the same number of inorganic ions with opposite charge to the bulk concentration of LiCl in water allows us to satisfy the global electroneutrality condition. Thus, the excess surface charge density in water is given by

$$\sigma_W = \int_{0}^{x_0} \sum_{i=Li^+,Cl^-} \rho_i(x) e z_i \mathrm{d}x = -\sigma_O. \quad (8)$$

If nitrobenzene is taken as a reference, we define the integrated excess surface charge density as

$$\sigma(x) = \int_{-x_0}^{x} \sum_i \rho_i(x) e z_i \mathrm{d}x, \quad (9)$$

for $i = \mathrm{TBA}^+$, TPB^-, Li^+, Cl^- and $x \leq x_0$. Applying the Gauss law, the electric field (perpendicular to the dielectric discontinuity) is given by

$$E(x) = \frac{\sigma(x)}{\varepsilon(x)\varepsilon_0}, \quad (10)$$

where $\varepsilon(x) = \varepsilon_O$ if $x < 0$ and $\varepsilon(x) = \varepsilon_W$ if $x > 0$. From this definition, the continuity of the perpendicular electric displacement

$$D_O^{\perp} = D_W^{\perp} = \lim_{x\to 0^-} \varepsilon_O E(x) = \lim_{x\to 0^+} \varepsilon_W E(x) \quad (11)$$

is fulfilled, in agreement with the Maxwell equations.[14,30] The difference in the mean electrostatic potential in the bulk phases of both immiscible electrolytes, $\Delta_O^W\Psi$, is calculated from the electric field as

$$\Delta_O^W\Psi = -\int_{-x_0}^{x_0} E(x)\mathrm{d}x. \quad (12)$$

Notice that a zero value in the bulk phase of nitrobenzene has been taken as a reference. The interfacial excess surface tension, $\gamma - \gamma_0$ (γ_0 is the surface tension at the point of zero charge), can then be obtained from the Lippmann equation (see eqn (1)).

II Results and discussion

In Fig. 2, experimental results of the excess surface tension at the nitrobenzene–water interface,[34] $\gamma - \gamma_0$, are collated with Monte Carlo results and theoretical calculations obtained *via* the non-linear Poisson–Boltzmann (NLPB) theory[29] for several electrolyte concentrations. In Fig. 2(A), the concentration of TBATPB ions in nitrobenzene is fixed and the concentration of LiCl ions in water is varied, while in Fig. 2(B) the opposite process is performed, that is, the concentration of LiCl ions in water is fixed and the concentration of TBATPB ions in nitrobenzene is varied. For all salt concentrations, Monte Carlo data agree with experimental results. The NLPB results resemble experimental data at low electrolyte concentrations, even though they deviate significantly at large values of the difference in the mean electrostatic potential in the bulk phases of the electrolytes, $\Delta_O^W\Psi$. These deviations are magnified at higher concentrations, contrasting with the good agreement between the Monte Carlo simulations and the experimental results.

In Fig. 3, the electric field and the ion distribution around the liquid interface are presented for several concentrations of LiCl ions in water, while the concentration of TBATPB ions in nitrobenzene is fixed. In Fig. 3(B), a positive excess surface charge density in oil, $\sigma_O > 0$, is considered, while the opposite value, $\sigma_W = -\sigma_O$, is considered in water. For all LiCl concentrations, the contact value of Cl^- is larger than the contact value of Li^+ (see Fig. 3(B)). This is consistent with the fact that the negative Cl^- ions are counterions of the positive excess surface charge in nitrobenzene, $\sigma_O > 0$. On the other hand, a very interesting behavior of the electric field in water can be observed in Fig. 3(A) when the concentration of LiCl increases. Near the dielectric discontinuity, the electric field peaks at the closest approach distance of Cl^- when the salt concentration of LiCl increases. As the dielectric constant is larger in water than in nitrobenzene ($\varepsilon_W > \varepsilon_O$), the electrostatic screening in water should be larger accordingly. Nevertheless, in Fig. 3(A) we observe that the magnitude of the electric field in water can be even larger than its maximum value in nitrobenzene for the highest salt concentration. This behavior can be understood noting that there is a significant amount of small positive Li^+ ions adsorbed to the dielectric interface at high electrolyte concentrations. These adsorbed cations, which are co-ions of the positive excess surface charge density in nitrobenzene,

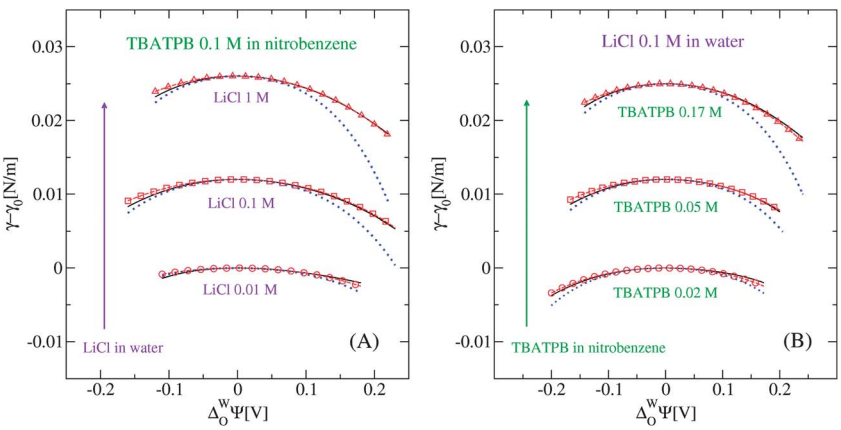

Fig. 2 Excess surface tension, $\gamma - \gamma_0$, at the oil–water interface as a function of the difference in the mean electrostatic potential in the bulk phases of both immiscible electrolytes, $\Delta_O^W\Psi$, for several electrolyte concentrations. γ_0 is the surface tension at the point of zero charge. In (A), the bulk concentration of TBATPB in nitrobenzene is 0.1 M in all instances, while the bulk concentration of LiCl in water is (from bottom to top) 0.01 M, 0.1 M, and 1 M. In (B), the bulk concentration of LiCl in water is 0.1 M in all cases, while the bulk concentration of TBATPB in nitrobenzene is (from bottom to top) 0.02 M, 0.05 M, and 0.17 M. Black solid and blue dotted lines correspond to the experimental electrocapillary data reported in ref. 34, and non-linear Poisson–Boltzmann calculations, respectively. Red empty symbols with dashed lines correspond to Monte Carlo simulation results. The excess surface tension is shifted for clarity.

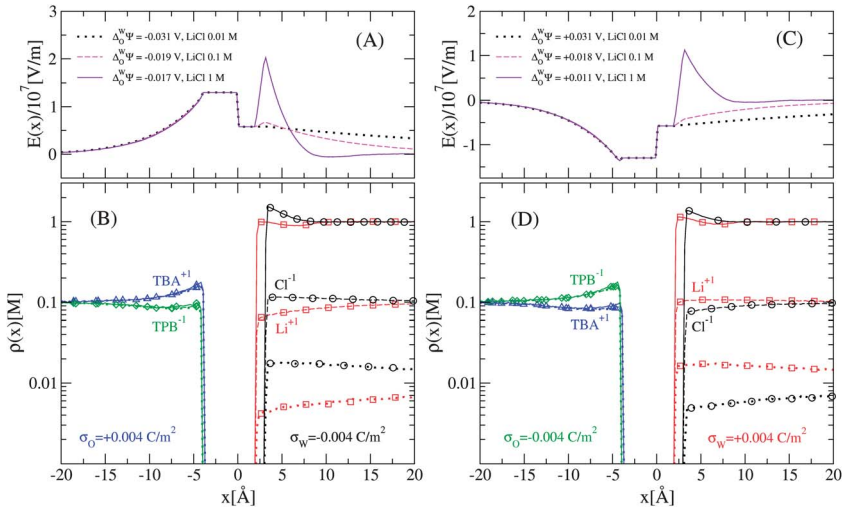

Fig. 3 Monte Carlo calculations of the electric field and ion distribution as a function of the distance to the oil–water interface. The bulk concentration of TBATPB in nitrobenzene is 0.1 M in all instances, while the bulk concentration of LiCl in water is 0.01 M (dotted lines), 0.1 M (dashed lines) and 1 M (solid lines) for all panels. In (B) and (D), Li^+, Cl^-, TBA^+, and TPB^- ions are represented by squares, circles, triangles, and diamonds, respectively. In (A) and (B), the excess surface charge density in water is negative, $\sigma_W = -0.004$ C m^{-2}, while in (C) and (D), the excess surface charge density in water is positive, $\sigma_W = +0.004$ C m^{-2}. The difference in the mean electrostatic potential in the bulk phases of both immiscible electrolytes, $\Delta_O^W\Psi$, is displayed in the insets of (A) and (C) for each ionic concentration.

$\sigma_O > 0$, enhance significantly the electric field in the aqueous phase near the liquid interface.

In Fig. 3(D), the ion profiles of organic and inorganic ions are displayed as a function of the distance to the dielectric discontinuity. In this case, a negative excess surface charge density in oil, $\sigma_O < 0$, is considered, while the opposite value, $\sigma_W = -\sigma_O$, is considered in water. For electrolyte concentrations 0.01 M and 0.1 M of LiCl, the contact values of Li^+ are larger than those of Cl^-. This is consistent with the fact that positive Li^+ ions are counterions of the negative excess surface charge density, $\sigma_O < 0$, in nitrobenzene. Nevertheless, at a concentration 1 M of LiCl, the previous trend inverts: the contact value of large Cl^- ions (co-ions of the negative excess surface charge in nitrobenzene, σ_O) is larger than the contact value of small Li^+ cations (which are the counterions of σ_O). The inversion of roles between counterions and co-ions is the so-called charge inversion.[20,35] The overcompensation of the negative excess surface charge in nitrobenzene promotes a reversal of the electric field in water, which peaks again at the closest approach distance of Cl^- (see Fig. 3(C)).

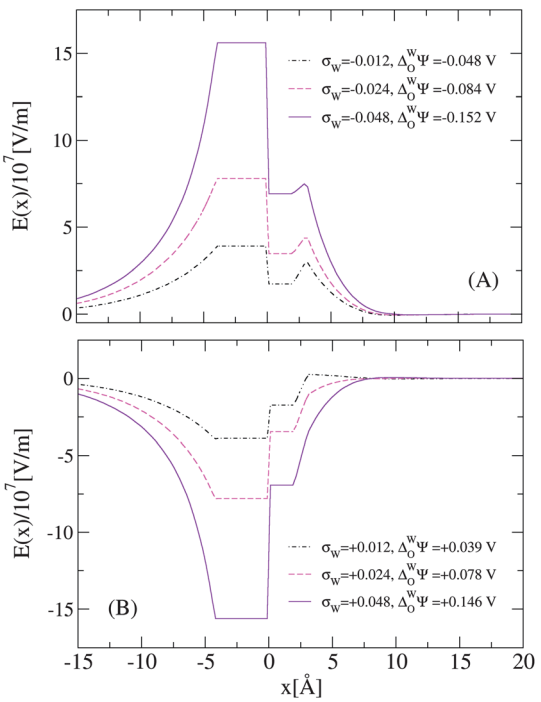

Fig. 4 Monte Carlo calculations of the electric field as a function of the distance to the oil–water interface for several excess surface charge densities, σ_W, in water. The bulk concentration of TBATPB in nitrobenzene is 0.1 M and the bulk concentration of the LiCl in water is 1 M, in both panels. The difference in the mean electrostatic potential in the bulk phases of both immiscible electrolytes, $\Delta_O^W\Psi$, is displayed in the insets of (A) and (B) for each excess surface charge density in water.

The significant adsorption of Li^+ ions to the liquid interface at high electrolyte concentrations is mainly due to the ionic size asymmetry and excluded volume effects (or depletion forces). This behaviour occurs for both polarities of the difference in the mean electrostatic potential in the bulk phases of the electrolytes, $\Delta_O^W\Psi$, in the presence of weak electric fields. Under these conditions, small cations (Li^+) can be significantly adsorbed to the liquid interface in a region that is not allowed to large anions (Cl^-) in water. If the smallest ions are counterions of the excess surface charge density in nitrobenzene, σ_O, this adsorbed layer of small counterions can overcompensate σ_O near the dielectric discontinuity, generating the so-called charge reversal[20] and the inversion of the electric field in the aqueous region (see Fig. 3(C)). In contrast, if the smallest ions are co-ions of σ_O then the net excess surface charge density in water can be larger than σ_O close to the dielectric discontinuity, producing the phenomenon of surface charge amplification[20] and the enhancement of the electric field (see Fig. 3(A)).

Finally, the interfacial behavior of the electric field for larger excess surface charge densities in water, σ_W, is displayed in Fig. 4(A) and (B). In order to facilitate the comparison of our results with future experimental data, the corresponding differences in the mean electrostatic potential in the bulk phases of both immiscible electrolytes, $\Delta_O^W\Psi$, are also displayed for each ionic concentration of LiCl in water. In Fig. 4(A), we observe that even though the enhancement of the electric field still persists for large negative differences of the mean electrostatic potential, $\Delta_O^W\Psi$, its magnitude is less pronounced. This means that the increase of positive excess charge in nitrobenzene increases the electrostatic repulsion exerted over Li^+ cations in water, thus gradually overcoming the attraction of Li^+ ions to the interface due to excluded volume effects. In contrast, Fig. 4(B) shows that the reversal of the electric field disappears at large positive differences in the mean electrostatic potential in the bulk phases of both immiscible electrolytes, $\Delta_O^W\Psi$.

III Conclusions

In this study, we provide an enhanced description of the ion distribution and the electric field near a liquid–liquid interface, including realistic ionic size-asymmetry, ion correlations, excluded volume of ions, and image charge effects *via* Monte Carlo simulations. This approach goes well beyond the classical Poisson–Boltzmann picture, in which such effects are completely neglected. The adequacy of this treatment is demonstrated *via* a comparison with experimental results of the excess surface tension at the nitrobenzene–water interface, without needing any adjustable parameter. We observe that the non-linear Poisson–Boltzmann theory is limited to low electrolyte concentrations, deviating significantly from experimental results in the opposite limit. We have also evinced that the ionic size-asymmetry and excluded volume effects play fundamental roles in the structure of the electrical double layer around a liquid–liquid interface at high electrolyte concentrations. In particular, we have shown that at a 1 M concentration of LiCl in water and a 0.1 M concentration of TBATPB in nitrobenzene, the significant adsorption of small Li^+ ions to the liquid interface is able to (i) enhance the electric field in the aqueous phase for positive excess surface charge densities in nitrobenzene and (ii) reverse the electric field in the aqueous phase for negative excess surface charge densities in nitrobenzene. These phenomena are analogous to the surface charge amplification and charge inversion reported by our research group in size-asymmetric electrolytes around a charged nanoparticle (even in the absence of image charge effects).[20] In that study, we showed that the surface charge amplification (or the adsorption of co-ions on the surface of a charged nanoparticle increasing its original bare charge) and the charge inversion (or the over-compensation of the original bare charge of the nanoparticle by counterions) can appear at high ion concentrations in the vicinity of the point of zero charge. We demonstrated that these effects are mainly driven by the ionic size asymmetry and excluded volume effects, and that they disappear at large valences of the nanoparticle. Here, we have shown that an analogous mechanism can produce the enhancement and the inversion of the electric field at a liquid interface near the point of zero charge (that is, for small differences in the mean electrostatic potential in the bulk phases of both immiscible electrolytes). These findings emphasize the relevance of the proper inclusion of ionic size-asymmetry, ion correlations and image charge effects in the description of the diffuse ionic distribution around charged surfaces and interfaces.

It is important to point out that these phenomena are not limited to occur only when an electric field is applied. The use of an electric field is one possibility to produce ionic charge accumulation at a liquid interface. In fact, such an ion distribution can also be induced by other mechanisms, such as ion partitioning, in which ions move from one liquid medium to another depending on their standard Gibbs energy of transfer[36] or *via* molecular pumps in cells.[37] These mechanisms are highly non-equilibrium processes since the ion's mobility and the resulting induced polarizability respond at different time scales.[38] As the distribution of ions around fluid interfaces is a common scenario in biological systems, our findings suggest that interesting phenomena such as the enhancement and reversal of the electric field, as well as the surface charge amplification[20,21] and charge inversion (already observed experimentally in macroscopic colloidal systems[22–25]) may also be present in nanoscopic biological liquid interfaces. We have also shown how the tuning of the electric field, enhancing or reversing its strength near the liquid interface, depends on the ion concentration and ionic size asymmetry. This suggests a new reversible physical mechanism to control the adsorption, self-assembly, and trapping/release of small charged nanoparticles, globular proteins, dendrimers or polyelectrolytes at the interface between two immiscible liquids in the presence of weak electric fields. Experimental techniques of atomic resolution[39–41] and recent theoretical improvements[42–44] will play an important role in gaining further insights into these phenomena at the molecular level.

Acknowledgements

This work was supported by the Nonequilibrium Energy Research Center, which is an Energy Frontier Research Center funded by the U.S. Department of Energy, Office of Science, Office of Basic Energy Sciences under Award Number DE-SC0000989. We also acknowledge the support of the AFOSR Award FA9550-10-1-0167 and the Quest computer cluster at Northwestern University.

References

1 L. Ramos, T. C. Lubensky, N. Dan, P. Nelson and D. A. Weitz, *Science*, 1999, **286**, 2325–2328.
2 E. Sanz, K. A. White, P. S. Clegg and M. E. Cates, *Phys. Rev. Lett.*, 2009, **103**, 255502.
3 D. Patra, A. Sanyal and V. M. Rotello, *Chem.–Asian J.*, 2010, **5**, 2442–2453.
4 R. Matsui, T. Sakaki and T. Osakai, *Electroanalysis*, 2012, **24**, 1164–1169.

5 J. S. Kim, L. He and J. J. Lemasters, *Biochem. Biophys. Res. Commun.*, 2003, **304**, 463–470.
6 K. M. Tyner, R. Kopelman and M. A. Philbert, *Biophys. J.*, 2007, **93**, 1163–1174.
7 J. C. Ojingwa and R. R. Isseroff, *J. Invest. Dermatol.*, 2003, **121**, 1–12.
8 B. E. Conway, *Electrochemical Supercapacitors: Scientific Fundamentals and Technological Applications*, Plenum Press, New York, 1999.
9 F. Reymond, D. Fermín, H. J. Lee and H. H. Girault, *Electrochim. Acta*, 2000, **45**, 2647–2662.
10 I. Benjamin, *Annu. Rev. Phys. Chem.*, 1997, **48**, 407–451.
11 E. J. W. Verwey and K. F. Niessen, *Philos. Mag.*, 1939, **28**, 435–446.
12 Y. Levin, *Rep. Prog. Phys.*, 2002, **65**, 1577–1632.
13 R. Messina, E. González-Tovar, M. Lozada-Cassou and C. Holm, *Europhys. Lett.*, 2002, **60**, 383–389.
14 D. Jackson, *Classical Electrodynamics*, John Wiley & Sons, New York, 1998.
15 Q. Cui, G. Zhu and E. Wang, *J. Electroanal. Chem.*, 1994, **372**, 15–19.
16 Q. Cui, G. Zhu and E. Wang, *J. Electroanal. Chem.*, 1995, **383**, 7–12.
17 L. I. Daikhin and M. Urbakh, *J. Electroanal. Chem.*, 2003, **560**, 59–67.
18 C. W. Monroe, M. Urbakh and A. A. Kornyshev, *J. Electroanal. Chem.*, 2005, **582**, 28–40.
19 D. Momotenko, C. M. Pereira and H. H. Girault, *Phys. Chem. Chem. Phys.*, 2012, **14**, 11268–11272.
20 G. I. Guerrero-García, E. González-Tovar and M. Olvera de la Cruz, *Soft Matter*, 2010, **6**, 2056–2065.
21 Z.-Y. Wang and Y.-Q. Ma, *J. Chem. Phys.*, 2010, **133**, 064704.
22 E. Raspaud, I. Chaperon, A. Leforestier and F. Livolant, *Biophys. J.*, 1999, **77**, 1547–1555.
23 K. Besteman, M. A. G. Zevenbergen, H. A. Heering and S. G. Lemay, *Phys. Rev. Lett.*, 2004, **93**, 170802.
24 M. Quesada-Pérez, E. González-Tovar, A. Martín-Molina, M. Lozada-Cassou and R. Hidalgo-Álvarez, *Colloids Surf., A*, 2005, **267**, 24–30.
25 F. H. J. van der Heyden, D. Stein, K. Besteman, S. G. Lemay and C. Dekker, *Phys. Rev. Lett.*, 2006, **96**, 224502.
26 Y. Marcus, *Chem. Rev.*, 1988, **88**, 1475–1498.
27 B. Krumgalz, *J. Chem. Soc., Faraday Trans. 1*, 1982, **78**, 437–449.
28 J. Koryta, P. Vanysek and M. Brezina, *J. Electroanal. Chem.*, 1977, **75**, 211–228.
29 W. Schmickler and E. Santos, *Interfacial Electrochemistry*, Springer-Verlag, Berlin, 2010.
30 G. M. Torrie and J. P. Valleau, *J. Electroanal. Chem.*, 1986, **206**, 69–79.
31 G. M. Torrie and J. P. Valleau, *J. Chem. Phys.*, 1980, **73**, 5807–5816.
32 D. Boda, K. Chan and D. Henderson, *J. Chem. Phys.*, 1998, **109**, 7362–7371.
33 G. I. Guerrero-García and M. Olvera de la Cruz, *J. Chem. Theory Comput.*, 2013, **9**, 1–7.
34 T. Kakiuchi and M. Senda, *Bull. Chem. Soc. Jpn.*, 1983, **56**, 1753–1760.
35 E. Wernersson, R. Kjellander and J. Lyklema, *J. Phys. Chem. C*, 2010, **114**, 1849–1866.
36 F. Reymond, *Transfer Mechanisms and Lipophilicity of Ionizable Drugs, Liquid Interfaces in Chemical, Biological, and Pharmaceutical Applications*, ed. A. G. Volkov, Marcel Dekker, New York, 2001.
37 B. I. H. Scott, *Annu. Rev. Plant Physiol.*, 1967, **18**, 409–418.
38 J. W. Zwanikken and M. Olvera de la Cruz, *Proc. Natl. Acad. Sci. U. S. A.*, 2013, **110**, 5301–5308.
39 E. Sloutskin, J. Baumert, B. M. Ocko, I. Kuzmenko, A. Checco, L. Tamam, E. Ofer, T. Gog, O. Gang and M. Deutsch, *J. Chem. Phys.*, 2007, **126**, 054704.
40 N. Laanait, J. Yoon, B. Hou, P. Vanysek, M. Meron, B. Lin, G. Luo, I. Benjamin and M. L. Schlossman, *J. Chem. Phys.*, 2010, **132**, 171101.
41 N. Laanait, M. Mihaylov, B. Hou, H. Yu, P. Vanysek, M. Meron, B. Lin, I. Benjamin and M. L. Schlossman, *Proc. Natl. Acad. Sci. U. S. A.*, 2012, **109**, 20326–20331.
42 S. Tyagi, M. Süzen, M. Sega, M. Barbosa, S. S. Kantorovich and C. Holm, *J. Chem. Phys.*, 2010, **132**, 154112.
43 V. Jadhao, F. J. Solis and M. Olvera de la Cruz, *Phys. Rev. Lett.*, 2012, **109**, 223905.
44 V. Jadhao, F. J. Solis and M. Olvera de la Cruz, *J. Chem. Phys.*, 2013, **138**, 054119.

